

Working memory and reward increase the accuracy of animal location encoding in the medial prefrontal cortex

Xiaoyu Ma¹, Charles Zheng², Yenho Chen², Francisco Pereira², Zheng Li^{1,*}

¹Section on Synapse Development Plasticity, National Institute of Mental Health, National Institutes of Health, 9000 Rockville Pike, Bethesda, MD 20892, United States,

²Machine Learning Team, National Institute of Mental Health, National Institutes of Health, 9000 Rockville Pike, Bethesda, MD 20892, United States

*Corresponding author: Section on Synapse Development Plasticity, National Institute of Mental Health, National Institutes of Health, Bethesda, MD 20892, United States. Email: lizheng2@mail.nih.gov

The ability to perceive spatial environments and locate oneself during navigation is crucial for the survival of animals. Mounting evidence suggests a role of the medial prefrontal cortex (mPFC) in spatially related behaviors. However, the properties of mPFC spatial encoding and how it is influenced by animal behavior are poorly defined. Here, we train the mice to perform 3 tasks differing in working memory and reward-seeking: a delayed non-match to place (DNMTP) task, a passive alternation (PA) task, and a free-running task. Single-unit recording in the mPFC shows that although individual mPFC neurons exhibit spatially selective firing, they do not reliably represent the animal location. The population activity of mPFC neurons predicts the animal location. Notably, the population coding of animal locations by the mPFC is modulated by animal behavior in that the coding accuracy is higher in tasks involved in working memory and reward-seeking. This study reveals an approach whereby the mPFC encodes spatial positions and the behavioral variables affecting it.

Key words: prefrontal cortex; reward; spatial encoding; working memory.

Introduction

Animals need to locate themselves in the environment to navigate safely, avoid predators, and forage for food. Perception of spatial location not only is critical for survival but also informs complex behaviors and high-level cognitive processes (Buzsáki and Moser 2013). Spatial locations can be represented by the firing of spatially tuned cells in rodents, such as place cells in the hippocampus. Spatially tuned cells are also present in human brains within the hippocampus and its surrounding medial-temporal-lobe areas (Ekstrom et al. 2003; Jacobs et al. 2013; Miller et al. 2013; Qasim et al. 2021).

Because the hippocampus is rich in spatial cells, it contributes to tasks reliant on spatial navigation. The medial prefrontal cortex (mPFC) has also been implicated in spatial navigation. However, these 2 regions focus on different aspects of spatial learning and memory. Although the hippocampus is required for spatial learning, the mPFC is involved in goal-directed actions, path planning, and strategy switching in spatial working memory tasks (Morris et al. 1982; Poucet and Buhot 1994; Ragozzino et al. 1999; Mumby et al. 2002; Hok et al. 2005; Yang and Mailman 2018; Kaefer et al. 2020). For example, lesioning or inactivating the hippocampus but not the mPFC leads to learning impairments in the rodent Morris water maze test; mPFC lesioning or inactivation impairs spatial working memory but not working memory for

visual objects or long-term spatial memory (Morris et al. 1982; Granon and Poucet 1995; Kesner et al. 1996; Yoon et al. 2008).

The mPFC in rodents is reciprocally connected to the mediodorsal nucleus of the thalamus (Krettek and Price 1977; Groenewegen 1988). The dorsal part of the mPFC comprises the frontal area 2 (Fr2) and dorsal anterior cingulate area (ACd), whereas the ventral part of the mPFC comprises prelimbic (PrL) and infralimbic (IL) areas (Uylings et al. 2003). Since the ventral mPFC is innervated by the ventral and intermediate hippocampus (Jay and Witter 1991; Cenquizca and Swanson 2007), the mPFC may represent animal location during spatial navigation as the hippocampus. This notion is supported by the finding of spatially selective firing of mPFC neurons (Jung et al. 1998; Spellman et al. 2015; Yang et al. 2014; Yang and Mailman 2018, but see Gemmell et al. 2002; Poucet 1997). However, unlike hippocampal place cells, mPFC neurons do not have the same sort of precise place fields or stable spatial firing rate maps, and the firing pattern of mPFC neurons often correlates with multiple features besides animal locations, such as goal locations, previous choices, environmental context, and task structures (Jung et al. 1998; Hok et al. 2005; de Saint et al. 2010; Hyman et al. 2012; Spellman et al. 2015; Ma et al. 2016). Moreover, mPFC neurons appear to exhibit spatially selective firing only during a working memory

task but not when animals simply search for randomly placed foods or explore the environment (Poucet 1997; Jung et al. 1998; Gemmell et al. 2002; Yang et al. 2014; Spellman et al. 2015). The mPFC may also use population activities to code the animal location. Indeed, it has been reported that the population activity of mPFC neurons occurring during coherent CA1-mPFC theta oscillations can be used to decode the animal location during a working memory task (Zielinski et al. 2019). It has yet to be determined if population coding of animal location is used specifically for working memory tasks and if it is influenced by other information processing activities of the brain during the task.

The goal of this study is to test whether working memory and reward influence the encoding of animal location in the mPFC. To address this question, we interrogated the properties of spatial encoding in the mPFC by recording mPFC neurons in several spatial tasks that have different requirements for working memory and reward-seeking. Our study shows that although individual mPFC neurons exhibit location-selective firing, their spatial tuning curves are broad. The population activity of mPFC neurons encodes the animal location more reliably. The accuracy of population coding is positively influenced by working memory and reward-seeking.

Materials and methods

Animals

Male C57BL/6 mice were purchased from The Jackson Laboratory. They were 8–12 weeks of age at first use. Mice were kept under a 12-h light (9 PM–9 AM)/dark (9 AM–9 PM) cycle. They were group-housed with littermates before surgery and singly housed after implantation of electrodes. Mice had ad libitum access to water and food before behavioral training. Two days before the training, mice were put under a water restriction protocol with only 1-h access to water every day. Their body weight was monitored daily to ensure it does not drop below 85% of the pre-water restriction baseline. All animal procedures followed the US National Institutes of Health Guidelines Using Animals in Intramural Research and were approved by the National Institute of Mental Health Animal Care and Use Committee.

Behavior

Behavioral training and testing were performed in a T-maze made of matte gray plexiglass under white light (70 lux). The maze was placed inside a grounded Faraday cage. The maze had a 40-cm-long center arm and two 35-cm-long branch arms. Each arm was 6-cm wide and 15-cm tall. There were 3 doors in the T-maze: The center door located 13-cm away from the end of the center arm, and the left and right doors were at the entrance of the left and right branch arms. There was a water spout at the end of each branch arm. The wall of the maze was decorated with visual cues. The maze was fitted with infrared emitter and sensor pairs

to detect when animals entered each arm and poked the water spout. The emitter and sensor pairs sent signals to a NI-DAQ USB-6212 Device controlled by Labview software (National Instruments, Austin, TX) to control door opening and water delivery.

DNMTP task

The animals were trained for the delayed non-match to place (DNMTP) task in 2 steps as described previously (Fuchs et al. 2007). In step 1, animals were trained to alternate the 2 branch arms to enter to receive water rewards. The center arm of the T-maze was blocked. Animals needed to alternate the water spouts in the 2 branch arms to poke to receive water rewards (~15- μ L drops). This step lasted for 3 days with a 20-min session on each day. All animals were able to receive water rewards by the end of the third day. In step 2, animals were trained to perform the DNMTP task. The DNMTP task started with the sample phase that was followed by the delay phase, then the test phase. At the beginning of the sample phase, the animal was released from the holding area and 1 of the 2 branch arms was randomly selected to be open. The animal received water rewards if it ran into the open arm and poked the water spout on the wall. The animal had to return to the holding area after getting the reward and be retained there for 10 s, which was the delay phase. The delay phase was followed by the test phase during which both branch arms were open. Once the animal passed a point in a branch arm that was 10-cm away from the intersection, the door to the other branch arm was closed. The animal received water rewards only if it entered the arm closed in the sample phase and poked the water spout. The intertrial interval was 40 s after the mouse made a correct choice in the test phase and extended to 70 s following trials with a wrong choice. We limited the maximum number of identical sample arms in a row to 3. The mice were trained for the DNMTP task for a 40-min session every day until they made $\geq 85\%$ correct choices in 3 consecutive days. Recordings on the third day were used for the analysis of correct-choice trials. For the analysis of wrong-choice trials, 9 recording sessions on the third day for animals who made wrong choice on this day and 2 sessions on the second day for the animals who did not make wrong choice on the third day were used. Only trials with correct choice were analyzed if not specified.

PA task

In the PA task, only 1 branch arm and the center arm were open. The open branch arm alternated between the right and left arms. The animal was released from the holding area into the open branch arm, received water rewards, then returned to the holding area and was retained there for 10 s. The recording session for the PA task was 20-min long.

Free-running

Animals run in the T-maze with water spouts blocked. In the first 10 min, only the right door was closed, and the animal explored the left and center arms. In the next 10 min, only the left door was closed, and the animal explored the right and center arms.

Fabrication of micro-drive electrode array

Fabrication of the micro-drive electrode array is similar as previously described (Zhang et al. 2016). A micro-drive was assembled from 3D-printed parts, screws, and nuts. Two nano-miniature connectors (Omnetics, Minneapolis, MN) were attached to the micro-drive with epoxy glue. Tetrodes were constructed from 4 twisted 19- μm Platinum 10% Iridium wires (California Fine Wire, Grover Beach, CA). A bundle of 16 tetrodes was attached to the micro-drive. The tetrode bundle can be advanced by turning the small screw on the micro-drive ($\sim 320 \mu\text{m}$ per turn). The impedance of each electrode measured after assembling was $\sim 1 \text{ M}\Omega$ at 1 kHz.

Surgery

Mice were anesthetized with isoflurane (3% for induction and 1% for maintenance) and placed on a stereotaxic frame (David Kopf Instruments, Tujunga, CA). The body temperature of the mouse was monitored and kept constant with a small-animal thermoregulation device. Craniotomies were made above the left or right mPFC (AP 1.8 mm and ML 0.4 mm). The electrodes were lowered into the mPFC (DV 1.8 mm). The gaps between the electrodes and craniotomies were filled with bone wax. Two skull screws were placed over the cerebellum and olfactory bulb to serve as ground and reference. The micro-drive was secured on the skull with dental cement. A piece of copper mesh was used to wrap the entire micro-drive, shielding electrical noise as well as protecting the micro-drive array from physical damage. Animals were allowed to recover for 2 weeks before being recorded.

In vivo recording

The nano-miniature connector was plugged into an RHD2132 amplifier connected to an RHD2000 USB interface board (Intan Technologies, Los Angeles, CA) through an extended cable. Electrical signals were filtered to obtain signals between 1 and 7,500 Hz, sampled and digitized at 30 kHz by the amplifier, and recorded by RHD2000 Interface software (Intan Technologies, Los Angeles, CA). The tetrodes were manually advanced $\sim 40\text{-}\mu\text{m}$ daily until more than half of the tetrodes detected clear neural firings. Recordings were then made at this location throughout the behavioral training and testing period. After the first round of behavior tests was completed, the tetrodes were further advanced for at least 200 μm to detect a new population of neurons. Mice with tetrodes no deeper than 2.4 mm after the final advancement were recorded during the second round of behavior testing. Animals were perfused and brains were

cut into 40- μm coronal sections with a cryostat to locate the recording site after all experiments were completed. Brain sections were stained with 0.5% cresyl violet and then imaged with a Nikon A1R microscope in the Systems Neuroscience Imaging Resource in the NIMH Intramural Research Program.

Data analysis

Single-unit isolation

The Offline Sorter software (Plexon, Dallas, TX) was used for spike detection and unit isolation. Spike sorting was performed as reported (Gray et al. 1995; Csicsvari et al. 1998). Briefly, the wideband signals were low-cut-filtered at 250 Hz. Putative waveforms passing a threshold of 3.5 noise sigma in at least 1 channel of the tetrode were detected, then sorted into single-unit clusters. Waveforms were sorted manually in a 3-dimensional feature space reflecting principal components, amplitudes, or energies of waveforms from the 4 channels of each tetrode. Only units containing at least 100 spikes in each session and having $<0.4\%$ of their spikes within the 2-ms refractory period were used for further analysis (Wilber et al. 2017). Units with an average firing rate of $<15 \text{ Hz}$ and a trough to peak waveform duration longer than 400 μs were considered to be putative principal cells (Frank et al. 2001). Neurons recorded in neighboring days were manually tracked according to their relative positions in a 3-dimensional feature space and then verified by computing similarities between the mean spike waveforms (Emondi et al. 2004).

Firing rate map construction

Animal locations were extracted with Top Scan software (Clever Sys, Reston, VA). The DNMTF trials were divided into 8 segments (SLF, SLB, SRF, SRB, TLF, TLB, TRF, and TRB) by task phase (S, sample phase and T, test phase), the branch arm that the mouse entered (L, left arm and R, right arm), and running direction (F, running forward towards the water spout; B, running back to the holding area). The PA and free-running trials were divided into 4 segments: LF (left forward), LB (left back), RF (right forward), and RB (right back).

The firing rate maps were constructed for each segment separately. We first excluded areas in which the animals regularly performed non-perambulatory behaviors (for example, drinking and grooming). These areas were generally within 5 cm of the water spout and in the holding area. Epochs during which the animal moved $<4 \text{ cm/s}$ were also removed from all analyses. The linear position of the mouse was measured as the distance in centimeters along the track from the center door. The trajectory was divided into 1.5-cm location bins, 45 bins in total. The firing rate within each location bin was calculated as the total number of spikes divided by the total time spent at that location bin across the entire session. The firing rate maps were smoothed with a Gaussian kernel (sigma = 2 location bins, Ciupek et al. 2015; Kee et al. 2018).

Population vector correlation

For each cell, all firing rates in the 2 segments to be compared were normalized by dividing them by the maximum firing rate of the cell. The normalized firing rate ranged from 0 to 1. Population vector in a certain location bin was generated from the firing rates of all cells in the bin. Pearson correlation coefficient between the population vectors of 2 segments was calculated for each location bin. The PVC for each segment pair was derived by averaging PVC across all bins in the segment.

To calculate intersegment PVC, the recording session containing multiple trials was randomly divided into 2 halves for 20 times. The firing rate map of each half was constructed and PVC between the 2 halves was calculated as intersegment PVC. The interbehavior PVC was calculated by averaging all intersegment PVCs.

Spatial information content

Spatial information content was calculated by using the previously reported formula (Skaggs et al. 1992):

$$\text{spatial information bit per spike} = \sum_{i=1}^N p_i \frac{\lambda_i}{\lambda} \log_2 \frac{\lambda_i}{\lambda}$$

where $i = 1, \dots, N$ represents location bin identification number, p_i is the probability of occupancy of bin i , λ_i is the mean firing rate of bin i , and λ is the overall mean firing rate of the cell in the maze.

Bayesian decoding

A Bayesian decoder (Mathis et al. 2012; Towse et al. 2014) was used to calculate the probability of the animal's presence in each location bin from the observed spikes. Animal location was decoded from the posterior probability matrix using a simple maximum likelihood method. Each segment was decoded separately.

Neural spikes during mouse running were binned into 200-ms nonoverlapping temporal bins. The spikes generated by N place cells during a time window T was $K = (k_1, \dots, k_i, \dots, k_N)$, where k_i was the number of spikes fired by the i th cell. The probability of observing K in time T given location x was taken as:

$$P(K|x) = \prod \text{Poisson}(k_i, T\alpha_i(x)) = \prod_{i=1}^N \frac{(T\alpha_i(x))^{k_i}}{k_i!} e^{-T\alpha_i(x)}$$

where x indexes the location bin defined in mouse trajectory and $\alpha_i(x)$ is the firing rate of the i th place cell at position x , derived from firing rate maps. The firing rate map was derived by using a cross-validation procedure, which excludes the currently decoding trial from the entire session.

Within each temporal bin, the animal location was decoded to the location bin with the highest posterior probability. Decoding performance was assessed from the average decoding error across the whole session. Decoding error was expressed as the absolute difference between the decoded position and true position. To account for the temporal bin difference between the

pair of segments or behaviors to be compared, the data set with more temporal bins were randomly resampled to have the same number of temporal bins as the other data set.

Data shuffling

The chance level of random spiking without relevance to the location was determined for each mouse with a random shuffling procedure. One thousand shuffles were performed for each cell in the sample. For each shuffled trial and each cell, the entire sequence of spikes fired by the cell was time-shifted along the animal's trajectory with a random interval drawn uniformly between 0 and the total trial length, and the end of the trial was wrapped to the beginning to allow for circular displacements (Langston et al. 2010). A permutation test was performed to compare original and shuffled data for each session.

Experimental design and statistical analyses

Seven of the 9 animals implanted with micro-drive arrays made $\geq 85\%$ correct choices in 3 consecutive days and they were included in electrophysiological recording. All 7 mice were used in the DNMTTP task. Six animals maintaining good quality of recording were advanced to the PA task and the free-running task. In 4 animals, the electrodes were advanced to a deeper location and recorded again after being recorded in all 3 tasks. Thus, we have 11 sessions in DNMTTP task, 10 sessions in PA task, and 10 sessions in the free-running task.

Sigma Plot software (Systat Software, Krakow, San Jose, CA) and Matlab (MathWorks, Natick, MA) were used for statistical analysis. When the data passed both normality and equal variance tests, comparisons between 2 groups were tested with 2-tailed, paired Student's t -test, and multi-group comparisons were conducted by using 1-way repeated measures analysis of variance (ANOVA) with post-hoc Bonferroni test. To compare 2 groups that failed normality test, equal variance test, or both, Wilcoxon signed-rank test was used. $P < 0.05$ was considered statistically significant.

Data and code accessibility

Data were analyzed with built-in or custom-built Matlab scripts. The Bayesian decoder Matlab scripts were adopted from Ólafsdóttir et al. (2016). The custom-built Matlab scripts and data are available upon request.

Results

The mPFC encodes animal location during a working memory task

Information in the brain can be represented by single-cells like hippocampal place cells, as well as by cell populations, such as engrams for memory (Hartley et al. 2014; Josselyn and Tonegawa 2020). We analyzed mPFC neurons at both the single-cell and population levels using tetrode recording. The recording was conducted in mice while they performed a DNMTTP task in a T-maze, a

spatial working memory test in which spatially selective firing of mPFC neurons has been detected (Spellman et al. 2015). The 2 branch arms of the T-maze were installed with water spouts at the end and the initial portion of the center arm was designated as a holding area. Access to the branch arms and the holding area was controlled by operating the entry doors. The DNMTTP task consisted of 3 phases: sample phase, delay phase, and test phase (Fig. 1A). In the sample phase, the animal was released from the holding area and a randomly selected branch arm was open. The animal received water rewards if it ran into the open branch arm and licked the water spout. The animal returned to the holding area after receiving rewards and was retained there for 10 s, which was the delay phase. The delay phase was followed by the test phase. Both branch arms were open in the test phase and the animal received water rewards only if it entered the arm closed in the sample phase and licked the water spout. The intertrial interval was 40 s for trials that mice made a correct choice in the test phase and 70 s for trials with a wrong choice.

Seven of the 10 trained mice reached the behavioral criterion within 10 days (Fig. 1C). The 3 underperformers were excluded from further testing. The electrodes in 4 of the 7 recorded mice were within 2 mm to the surface of the cortex. They were advanced for at least an additional 200 μm after recording at their initial locations to reach different groups of neurons. A distinct group of neurons was recorded during each recording session. The final positions of the electrode tips were shown in Supplementary Fig. 1. We recorded a total of 11 sessions in 7 mice wherefrom 596 single units were isolated. Of the single units, 541 were identified as putative principal neurons and 55 as putative non-principal neurons by waveform features. Since the small number of non-principal neurons limited statistical power, our analysis was focused on principal neurons.

To assess the relation between neural firing and behavioral state, we divided each DNMTTP trial into 8 segments (SLF, SLB, SRF, SRB, TLF, TLB, TRF, and TRB) by task phase (S, sample phase; T, test phase), the branch arm that the mouse entered (L, left arm; R, right arm), and running direction (F, running forward towards the water spout; B, running back to the holding area). We constructed a firing rate map for each cell. Some mPFC neurons showed location-selective firing (Fig. 1D–F). To compare the same neuron's firing rate maps in different segments, we ordered all cells by their peak firing positions in the SLF segment, then used the obtained cell order to arrange cells for the TLF, SRF, and SLB segments (Fig. 1F). The composite firing rate map of each segment was distinct, suggesting that the peak firing position of individual mPFC neurons is variable across task segments. We further assessed this variation by computing a population vector for each location from all recorded principal cells' firing rates. The correlation of population vectors (PVC) between segments with the same features (within-segment) was

0.51 ± 0.02 , which was significantly above the chance level obtained by shuffling the data to decouple neural spiking from animal locations (the mean of shuffled data, 0.24 ± 0.02 ; paired *t*-test, $t_{10} = 18.58$, $P = 4.41 \times 10^{-9}$; $n = 11$ sessions; $P < 0.001$ for the permutation test of each session). PVC between the “sample” and “task” segments with same running directions and branch arms was comparable to that for within-segment (1-way repeated measures ANOVA, $f = 131.65$, $P = 9.80 \times 10^{-11}$; post-hoc Bonferroni test, $P = 0.11$; $n = 11$ sessions; Fig. 1G and H). PVC between forward and back segments was lower than the within-segment PVC (post-hoc Bonferroni test, $P = 9.22 \times 10^{-7}$; $n = 11$ sessions; Fig. 1G and H). Although PVC between the left and right segments was comparable to the within-segment PVC in the center arm (post-hoc Bonferroni test, $P = 0.54$; $n = 11$ sessions; Fig. 1G and H), it was reduced in the branch arm (post-hoc Bonferroni test, $P = 1.27 \times 10^{-4}$; $n = 11$ sessions; Fig. 1G and H). These findings suggest that animal location and running direction affect mPFC neurons' spiking activities.

To further assess the spatially related activity of mPFC neurons, we calculated the spatial information content of each neuron as previously reported (Skaggs et al. 1992). Although the spatial information content was comparable between sample and test segments (Wilcoxon signed-rank test, $z = 0.48$, $P = 0.63$, and $n = 541$ neurons; Fig. 1I) and between left and right segments (Wilcoxon signed-rank test, $z = -1.43$, $P = 0.15$, and $n = 541$ neurons; Fig. 1I), it was higher in forward segments than in back segments (Wilcoxon signed-rank test, $z = -3.85$, $P = 1.19 \times 10^{-4}$, and $n = 541$ neurons; Fig. 1I). The mean firing rate was comparable in all segments (Wilcoxon signed-rank test, sample vs. test, $z = -1.36$, $P = 0.17$; left vs. right, $z = 0.55$, $P = 0.58$; forward vs. back, $z = 0.94$, $P = 0.35$; and $n = 541$ neurons; Fig. 1J). These results indicate that mPFC neuron spiking contains more spatial information during running towards the water spout than during running back to the holding area.

Although an individual mPFC neuron's firing contains spatial information, itself was not a reliable predictor of animal location as it varied with trials (Fig. 1E, G, and H). Next, we tested whether the population activity of mPFC neurons can be used to decode the animal location. We used a Bayesian decoder (Towse et al. 2014) to infer the animal position from the spiking of all recorded principal neurons. We were able to decode the animal position with a decoding error (expressed as the distance between the animal's actual and decoded locations) well below the chance level (paired *t*-test, $t_{10} = -30.327$, $P = 3.56 \times 10^{-11}$; and $n = 11$ sessions; Fig. 1K and L; and $P < 0.001$ for the permutation test of each session). Although the decoding error was comparable between sample and test segments (paired *t*-test, $t_{10} = 0.56$, $P = 0.59$; and $n = 11$ sessions) and between left and right segments (paired *t*-test, $t_{10} = 1.48$, $P = 0.170$; and $n = 11$ sessions), it was smaller in forward than in back segments (paired *t*-test, $t_{10} = -3.863$, $P = 0.003$; and $n = 11$ sessions; Fig. 1M). These results

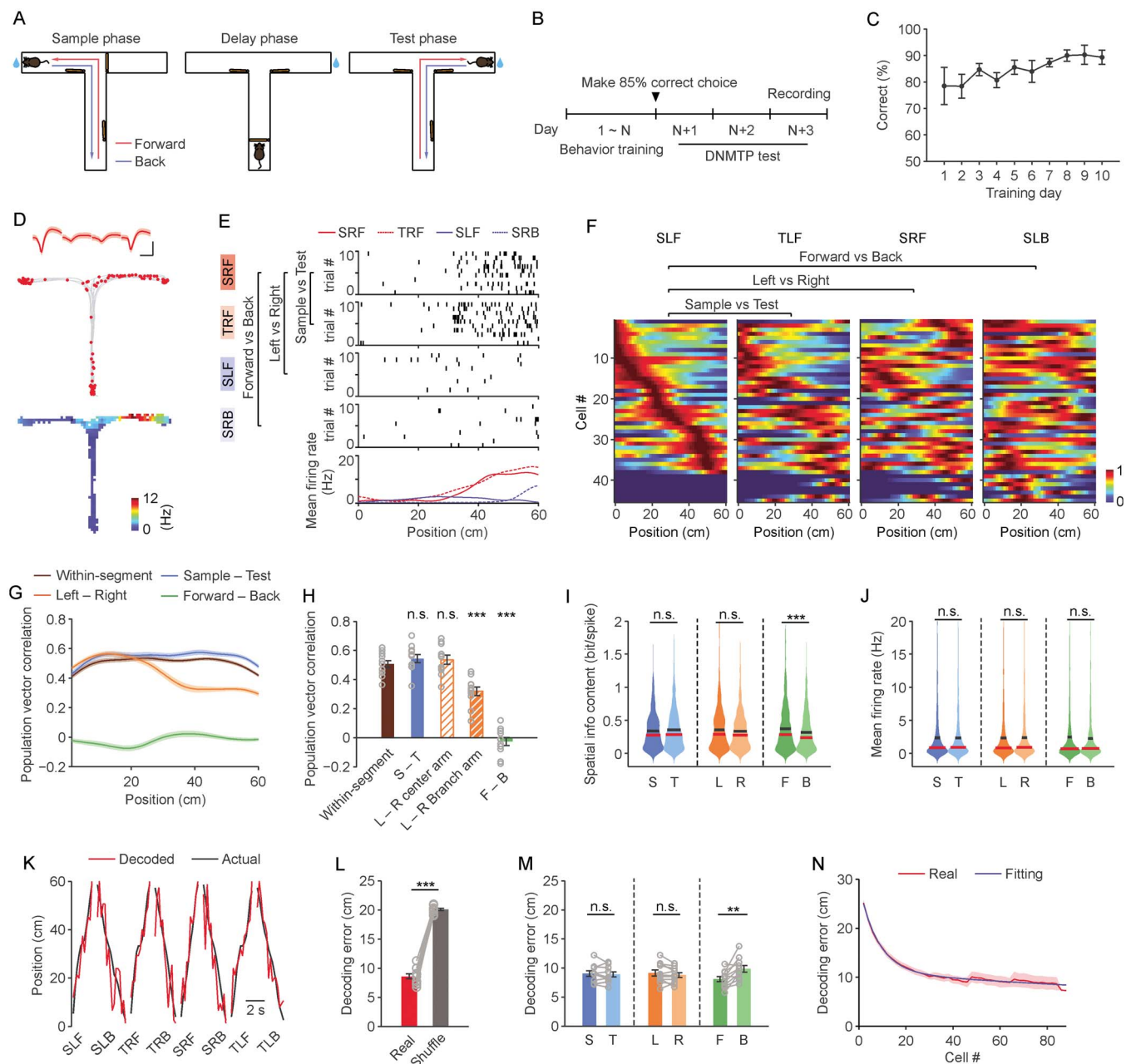


Fig. 1. Spatially biased firing of mPFC neurons in the DNMTT task. Mice of 8-week old were implanted with a bundle of tetrodes in the mPFC and trained in the T-maze for the DNMTT task 2 weeks later. A) Diagram of the DNMTT task. B) Experimental schedule. C) The animal's performance during training for the DNMTT task; $n = 7$ mice. D) Representative trajectory of an animal (gray lines), firing location of a neuron in this animal (red dots), and the mean firing rate map of the neuron. The waveform of the neuron is shown on top as mean \pm SEM. Scale bars: time, 500 μ s; voltage, 40 μ V. E) Representative raster plots of neural spiking (top 4 graphs) and mean firing rate during different task segments (bottom graph) of 1 neuron. X-axis indicates the animal's position represented by the distance to the holding area. F) Representative composite firing rate map of all neurons recorded in 1 animal. The cells were ordered by their peak firing locations in the SLF segment. Color in the firing rate map indicates normalized firing rates. G) PVC between different trials of the same segment (within-segment) and between different task segments at each position. Lines indicate the average PVC from 11 sessions from 7 mice. H) PVC averaged across all positions for the within-segment, sample vs. task, and forward vs. back comparison, and across the positions in the center or branch arm for the left vs. right comparison. Each circle represents 1 session; $n = 11$ sessions from 7 mice. I) Spatial information content and J) mean firing rate of all neurons in designated task segments presented as violin plots illustrating kernel probability density, i.e. the width of the outlined area represents the proportion of the data located there. Red line is median and black line is mean; $n = 541$ neurons from 7 mice. K) Representative actual (black) and decoded (red) animal positions in each task segment in 1 animal. L) Decoding error resulting from using recorded neural spiking and shuffled spiking data. Each circle represents 1 session; $n = 11$ sessions from 7 mice. M) Decoding error of designated task segments. Each circle represents 1 session; $n = 11$ sessions from 7 mice. N) Decoding error as a function of the number of neurons used in decoding. Data are presented as mean \pm SEM in C, G, H, L-N). ** $P < 0.01$ and *** $P < 0.001$.

indicate that the population activity of mPFC neurons represents the animal location and that the coding accuracy is higher during running towards rewards than during running back.

To examine the relation between the number of mPFC neurons and coding accuracy, we decoded animal locations from randomly selected subsets of recorded cells with different cell numbers. The resulting decoding error

vs. cell number plot can be fitted with a 2-term exponential function with $\tau_1 = 8.0$ and $\tau_2 = 324.0$. The fitted curve had a steep downward trend before the neuron number reached ~ 20 (Fig. 1N). Adding more neurons after this point only slightly decreased decoding error (Fig. 1N).

The above decoding was based on trials that the animal made correct choice. We also examined the coding of animal locations in the wrong-choice trials. The decoding error was significantly higher in wrong-choice trials than in correct-choice trials (paired t-test, $t_{10} = 2.47$, $P = 0.033$; and $n = 11$ sessions; Supplementary Fig. 2), but it was still much lower than the chance level (paired t-test, $t_{10} = -10.56$, $P = 9.62 \times 10^{-7}$, and $n = 11$ sessions).

Taken together, these findings show that although the spikes of individual mPFC neurons contain spatial information, the population activity of mPFC neurons encodes animal location in the DNMTTP task more reliably than single-cell spiking. The population encoding has a higher accuracy during running to retrieve rewards than after receiving rewards.

Spatial encoding in the mPFC is enhanced by working memory

The DNMTTP task is a working memory test (Rawlins and Olton 1982; Korotkova et al. 2010). To test for the effect of working memory on mPFC's spatial encoding, we designed a passive alternation (PA) task in which the animal alternated the 2 branch arms to enter without having to use working memory (Fig. 2A). In each trial, one of the branch arms was open, the animal ran into it to receive water rewards, then returned to the holding area. After the animal was retained in the holding area for 10 s, only the other branch arm was opened to allow the animal to enter and receive water rewards. The intertrial interval was 10 s.

The PA test was conducted on the day after recording in the DNMTTP task (Fig. 2B). Five hundred twenty four putative principal neurons were isolated from recordings of 10 sessions in 6 mice during the PA task. Since the PA task had no sample or test phase, it was divided into 4 segments (LF, LB, RF, and RB) by the branch arm entered (L/R) and running direction (F/B). mPFC neurons exhibited location-selective firing in the PA task as in the DNMTTP task (Fig. 2C). The firing rate map was different between the left and right segments and between the forward and back segments as revealed by PVC (1-way repeated measures ANOVA, $f = 139.36$, $P = 9.04 \times 10^{-13}$; post-hoc Bonferroni test: between left and right in branch arm vs. within-segment, $P = 0.006$; between forward and back vs. within-segment, $P = 6.84 \times 10^{-7}$; and $n = 10$ sessions; Fig. 2D–F).

Spatial information content was comparable in left and right segments (Wilcoxon signed-rank test, $z = -0.80$, $P = 0.42$; and $n = 524$ neurons), but was higher in forward than in back segments (Wilcoxon signed-rank test, $z = -4.84$, $P = 1.30 \times 10^{-6}$; and $n = 524$ neurons; Fig. 2G). The mean firing rate was indistinguishable between segments (Wilcoxon signed-rank test: left vs.

right, $P = 0.65$; forward vs. back, $P = 0.26$; and $n = 524$ neurons; Fig. 2H). We were able to decode the animal location from the population activity of recorded neurons by using the Bayesian decoder (paired t-test, $t_9 = -18.12$, $P = 2.16 \times 10^{-8}$; and $n = 10$ sessions; $P < 0.001$ for the permutation test of each session; Fig. 2I). The decoding error for left and right segments was similar (paired t-test, $t_9 = 0.53$, $P = 0.61$; and $n = 10$ sessions), but lower for forward than for back segments (paired t-test, $t_9 = -3.32$, $P = 0.009$; and $n = 10$ sessions; Fig. 2J). The curve for decoding error vs. cell number can be fitted with a 2-term exponential function ($\tau_1 = 11.5$ and $\tau_2 = 304.9$; Fig. 2K).

To test for the effect of working memory on spatial encoding, we examined neurons that were recorded during both PA and DNMTTP. These neurons exhibited different firing rate maps in the DNMTTP and PA tasks (Fig. 3A and B) and a lower PVC between DNMTTP and PA than that between segments within the same task (1-way repeated measures ANOVA, $f = 180.01$, $P = 6.63 \times 10^{-10}$; post-hoc Bonferroni test: within-DNMTTP vs. within-PA, $P = 0.092$; within-DNMTTP vs. between DNMTTP and PA, $P = 7.50 \times 10^{-8}$; within-PA vs. between DNMTTP and PA, $P = 1.68 \times 10^{-6}$; $n = 10$ sessions; Fig. 3C and D). The spatial information content of the same mPFC neurons was higher in the DNMTTP task than in the PA task (Wilcoxon signed-rank test, $z = -3.54$, $P = 4.07 \times 10^{-4}$; and $n = 319$ neurons; Fig. 3E). There was no significant difference between the DNMTTP and PA tasks in the mean firing rate (Wilcoxon signed-rank test, $z = 1.39$, $P = 0.16$; and $n = 319$ neurons; Fig. 3F). The decoding error for animal locations from the same population of neurons was lower in the DNMTTP task than in the PA task (paired t-test, $t_9 = -3.445$, $P = 0.007$, and $n = 10$ sessions; Fig. 3G).

Taken together, these results indicate that the spikes of mPFC neurons contain more spatial information and that mPFC neural populations encode animal locations with higher accuracy in the DNMTTP than in the PA task. Hence, working memory increases mPFC's spatial encoding capability.

Spatial encoding in the mPFC is enhanced by reward

Both the DNMTTP and PA testing showed that the spikes of mPFC neurons contain more spatial information and that the mPFC better encodes animal location in forward segments than in back segments. Forward and back segments differed in reward status with the reward being a goal in forward segments and a past event in back segments. To test whether reward affects the spatial encoding of mPFC neurons, we conducted a free-running task in which animals run in the T-maze with only 1 branch arm open and all water spouts blocked (Fig. 4A). The free-running task was similar to the PA task except for the lack of reward. The animal first explored the left and center arms for 10 min, then the right and center arms for 10 min. Animals were recorded in the free-running task on the day after PA testing (Fig. 4B).

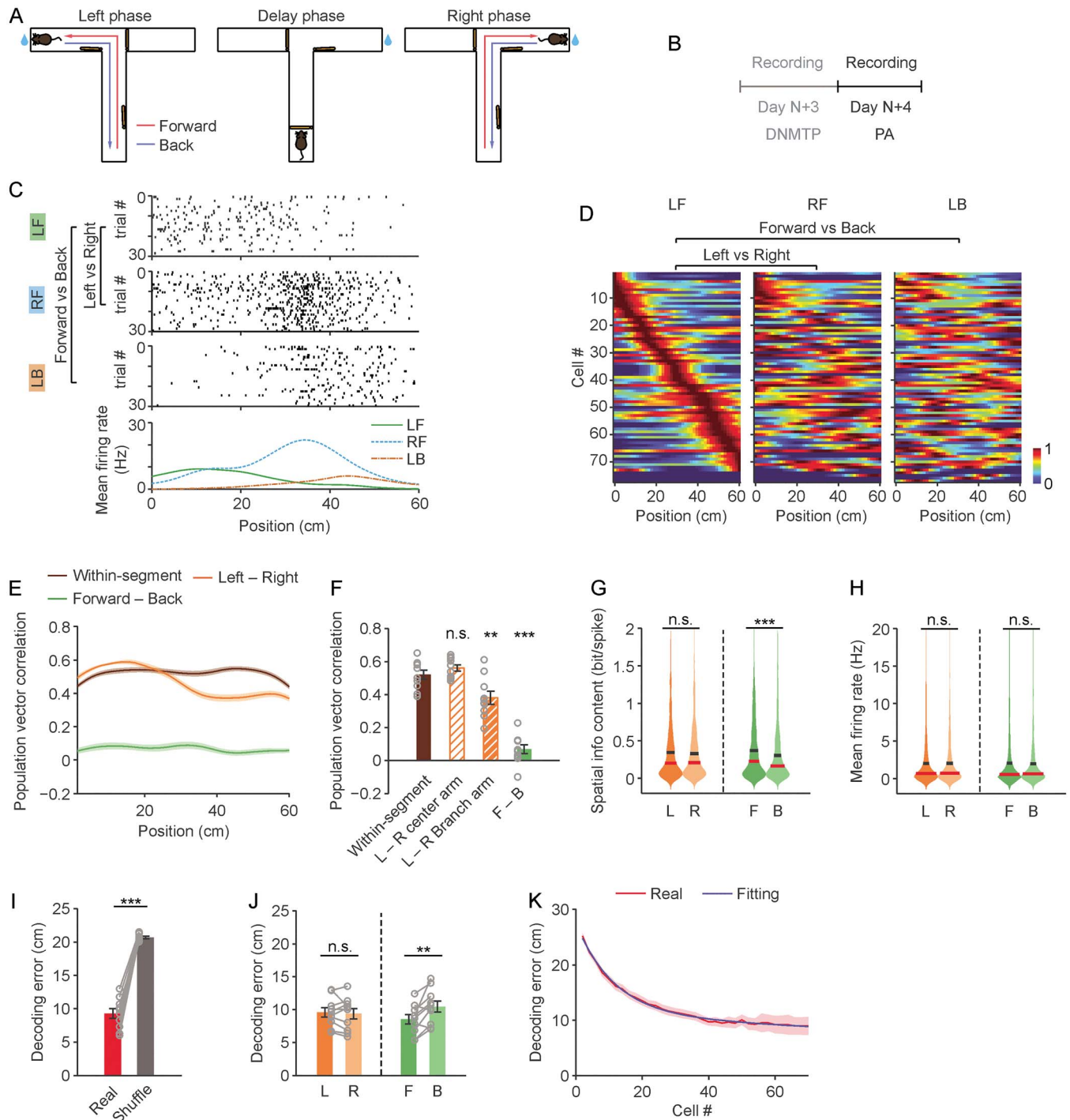


Fig. 2. Spatially biased firing of mPFC neurons in the PA task. Mice were recorded in the PA task on the day after they were recorded in the DNMTTP task. A) Diagram of the PA task. B) Experimental schedule. C) Representative raster plots of neural spiking (top 3 graphs) and mean firing rate during different task segments (bottom graph) of 1 neuron. X-axis indicates the animal's position represented by the distance to the holding area. D) Representative composite firing rate map of all neurons recorded in 1 animal. The cells were ordered by their peak firing locations in the LF segment. Color in the firing rate map indicates normalized firing rates. E) PVC between different trials of the same segment (within-segment) and between different task segments at each position of a task segment. Lines indicate the average PVC from 10 sessions from 6 animals. F) PVC averaged across all positions for the within-segment and forward vs. back comparison, and across the positions in the center or branch arm for the left vs. right comparison. Each circle represents 1 session; $n = 10$ sessions from 6 mice. G) Spatial information content and H) mean firing rate of all neurons in designated task segments presented as violin plots illustrating kernel probability density. Red line is median and black line is mean; $n = 524$ neurons from 6 mice. I) Decoding error resulting from using recorded neural spiking and shuffled spiking data. Each circle represents 1 session; $n = 10$ sessions from 6 mice. J) Decoding error of designated task segments. Each circle represents 1 session; $n = 10$ sessions from 6 mice. K) Decoding error as a function of the number of neurons used in decoding. Data are presented as mean \pm SEM in E, F, I-K). ** $P < 0.01$ and *** $P < 0.001$.

mPFC neurons displayed spatially biased firing during the free-running task (Fig. 4C and D). Like in the DNMTTP and PA tasks, PVC between the left and right

segments in the branch arms as well as PVC between forward and back segments were lower than the within-segment PVC (1-way repeated measures ANOVA,

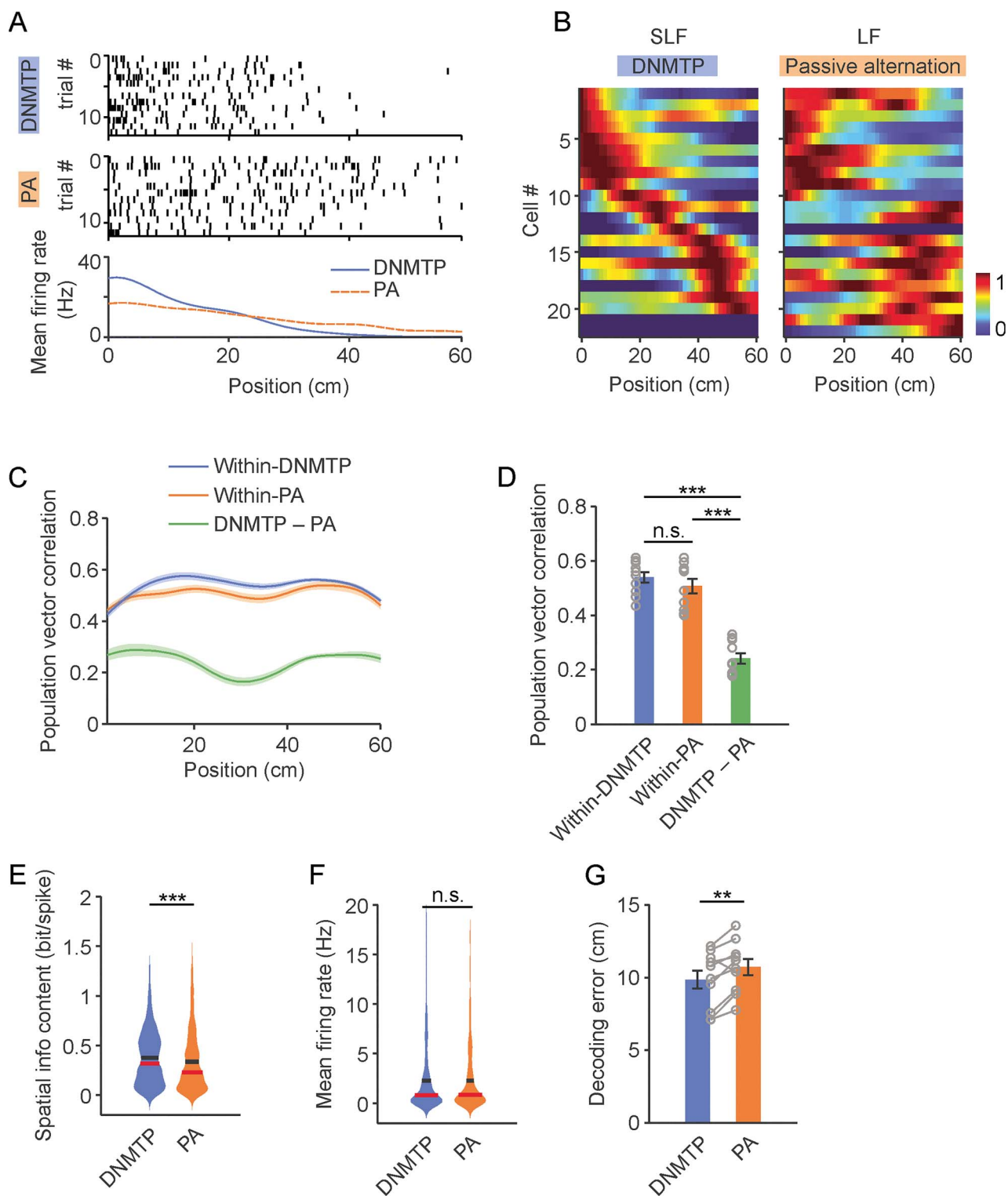


Fig. 3. The effect of working memory on the spatial encoding of mPFC neurons. Spatial encoding was compared in neurons tracked in the DNMT and the PA task. **A**) Representative raster plots of neural spiking (top 2 graphs) and mean firing rate during different tasks (bottom graph) of 1 neuron. X-axis indicates the animal's position represented by the distance to the holding area. **B**) Representative composite firing rate map of all neurons recorded in 1 animal, which are tracked in DNMT and PA task. The cells were ordered by their peak firing locations in the DNMT task. Color in the firing rate map indicates normalized firing rates. **C**) PVC between different trials of the same task (within-DNMT and within-PA) and between the DNMT and the PA task at each position. Lines indicate the average PVC from 10 sessions from 6 mice. **D**) PVC averaged across all positions for the within-DNMT, within-PA, and between DNMT and PA comparison. Each circle represents 1 session; $n = 10$ sessions from 6 mice. **E**) Spatial information content and **F**) mean firing rate of all neurons in designated tasks presented as violin plots illustrating kernel probability density. Red line is median and black line is mean; $n = 319$ neurons from 6 mice. **G**) Decoding error of DNMT and PA task. Each circle represents 1 session; $n = 10$ sessions from 6 mice. Data are presented as mean \pm SEM in **C**, **D**, and **G**. ** $P < 0.01$ and *** $P < 0.001$.

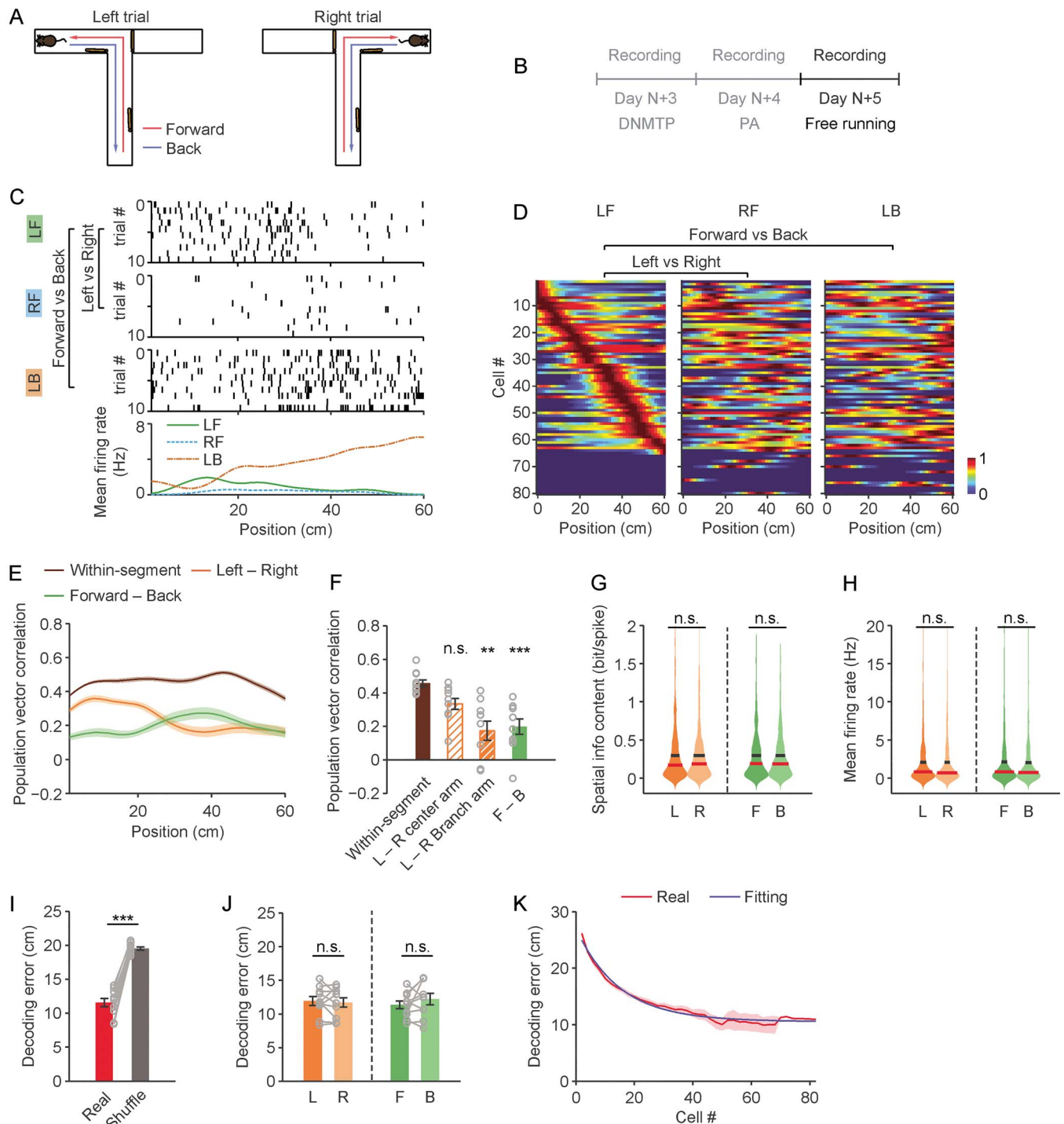


Fig. 4. Spatially biased firing of mPFC neurons during animal free-running in T-maze. Mice were recorded in the free-running on the day after they were recorded in the PA task. A) Diagram of the free-running. B) Schedule of behavioral training. C) Representative raster plots of neural spiking (top 3 graphs) and mean firing rate during different task segments (bottom graph) of 1 neuron. D) Representative composite firing rate map of all neurons recorded in 1 animal. The cells were ordered by their peak firing locations in the LF segment. Color in the firing rate map indicates normalized firing rates. E) PVC between different trials of the same segment (within-segment) and between different task segments at each position. Lines indicate the average PVC from 10 sessions from 6 mice. F) PVC averaged across all positions for the within-segment and forward vs. back comparison, and across the positions in the center or branch arm for the left vs. right comparison. Each circle represents 1 session; $n = 10$ sessions from 6 mice. G) Spatial information content and H) mean firing rate of all neurons in designated task segments presented as violin plots illustrating kernel probability density. Red line is median and black line is mean; $n = 470$ neurons from 6 mice. I) Decoding error resulting from using recorded neural spiking and shuffled spiking data. Each circle represents 1 session; $n = 10$ sessions from 6 mice. J) Decoding error of designated task segments. Each circle represents 1 session; $n = 10$ sessions from 6 mice. K) Decoding error as a function of the number of neurons used in decoding. Data are presented as mean \pm SEM in E, F, I-K). ** $P < 0.01$ and *** $P < 0.001$.

$f = 16.96$, $P = 2.32 \times 10^{-5}$; post-hoc Bonferroni test: between left and right in branch arm vs. within-segment, $P = 0.003$; between forward and back vs. within-segment, $P = 1.74 \times 10^{-4}$; and $n = 10$ sessions; Fig. 4E and F). The mean firing rate was comparable between segments (Wilcoxon signed-rank test: left vs. right, $z = -0.58$, $P = 0.56$; forward vs. back, $z = -1.89$, $P = 0.059$; and $n = 470$ neurons; Fig. 4H).

However, unlike the DNMT and PA tasks, individual neurons' spatial information contents and the decoding error of animal location from population activities were comparable in all task segments (Spatial information content: left vs. right, $z = -0.59$, $P = 0.555$; forward vs. back, $z = -0.17$, $P = 0.866$; $n = 470$; Wilcoxon signed-rank test. Decoding error: left vs. right, $t_9 = 0.46$, $P = 0.66$; forward vs. back, $t_9 = -1.24$, $P = 0.25$; $n = 10$ sessions; paired t-test; Fig. 4G, I–K).

To test for the effect of reward on spatial encoding, we examined neurons that were recorded in both the PA and free-running tasks. PVC between PA and free-running was lower than that of within-task segments (1-way repeated measures ANOVA, $f = 92.6$, $P = 3.85 \times 10^{-10}$; post-hoc Bonferroni test: between PA and free-running vs. within-PA, $P = 2.01 \times 10^{-6}$; between PA and free-running vs. within-free-running, $P = 4.45 \times 10^{-6}$; $n = 10$ sessions; Fig. 5A–D), indicating that the same neuron has different firing rate maps in PA and free-running tasks. The spike of mPFC neurons contained more spatial information (Wilcoxon signed-rank test, $z = -2.94$, $P = 0.003$; and $n = 313$ neurons; Fig. 5E), and the mPFC population activity encoded the animal location with smaller errors (paired t-test, $t_9 = -3.52$, $P = 0.007$; and $n = 10$ sessions; Fig. 5G) in PA than in free-running testing. The mean firing rate was lower during the PA than during the free-running task (Wilcoxon signed-rank test, $z = 2.28$, $P = 0.022$; and $n = 313$ neurons; Fig. 5F).

To test whether distance to the reward location affects mPFC spatial encoding, we divided the forward segments of all 3 tasks into 2 parts of equal length, one proximal to the reward and the other one distal to the reward, then calculated decoding error for each part separately. Decoding error was significantly larger in the distal part than in the proximal part during the DNMT and PA tasks (paired t-test: $t_{10} = 2.95$, $P = 0.015$, and $n = 11$ sessions in DNMT; $t_9 = 3.70$, $P = 0.005$, and $n = 10$ sessions in PA; Supplementary Fig. 3A and B), but it was comparable in the 2 parts during free-running, which was not provided with rewards (paired t-test, $t_9 = 1.34$, $P = 0.21$; and $n = 10$ sessions; Supplementary Fig. 3C). These findings indicate that location decoding is more accurate when the animal is closer to rewards.

Taken together, these findings indicate that reward increases individual neurons' spatial information contents and the neural population's spatial encoding accuracy in the mPFC.

Discussion

The mPFC receives a broad range of sensory, spatial, and emotional information and has been implicated in such high-level cognitive functions as executive control, decision making, attention, and emotional regulation (Euston et al. 2012; Dixon et al. 2017). In this study, we examined the properties of spatial encoding in the mPFC during different behavioral tasks. Our results show that the population activity of mPFC neurons encodes the animal location regardless of working memory and rewards. However, working memory and reward-seeking increase coding accuracy and the spatial information content of neural spikes.

Some studies have detected spatially selective firing of mPFC neurons. Jung et al. reported that a small number of mPFC neurons display arm-specific firing in an 8-arm radial maze test or have higher firing rates on one side of the track in a figure-8-track test (Jung et al. 1998). Spellman et al. and Yang et al. found that mPFC neurons can distinguish the left and right goal arms in a spatial delayed alternation task (Yang et al. 2014; Spellman et al. 2015). Poucet and Gemmell reported that the firing of mPFC neurons in non-working memory tasks is not place-selective (Poucet 1997; Gemmell et al. 2002); these findings, however, need validation with larger sample sizes as only a small number of cells were recorded in these studies (31 and 42 cells). In addition to the ambiguity in the literature about the existence of spatially selective mPFC neurons, even fewer studies are on population coding of spatial position in the mPFC.

We recorded single units in the mPFC of mice while they performed a DNMT task to receive water rewards by using working memory. We used the PVC analysis to compare the spatial firing rate maps of mPFC neurons in different branch arms, task phases, running direction, and reward status. When comparing the right and left segments, PVC for the branch arm was lower than that for the center arm. This finding suggests that there is a behavioral state-independent component in the spatially biased firing of mPFC neurons as animals were in the same task phase, running direction, and reward status in the center and branch arms. Although the task phase has a limited effect on the spatially selective firing of mPFC neurons, running direction and/or reward status appear to have significant effects as PVC between forward and back segments was low.

Forward and back segments may also have different working memory loads besides reward status and running direction. We used the PA and free-running tasks to tease apart their effects. Although the PA task is rewarded as the DNMT task, it does not require working memory. The free-running task involves neither working memory nor reward. PVC for the same neuronal population in the same maze between DNMT and PA tasks and that between PA and free-running tasks was low, indicating

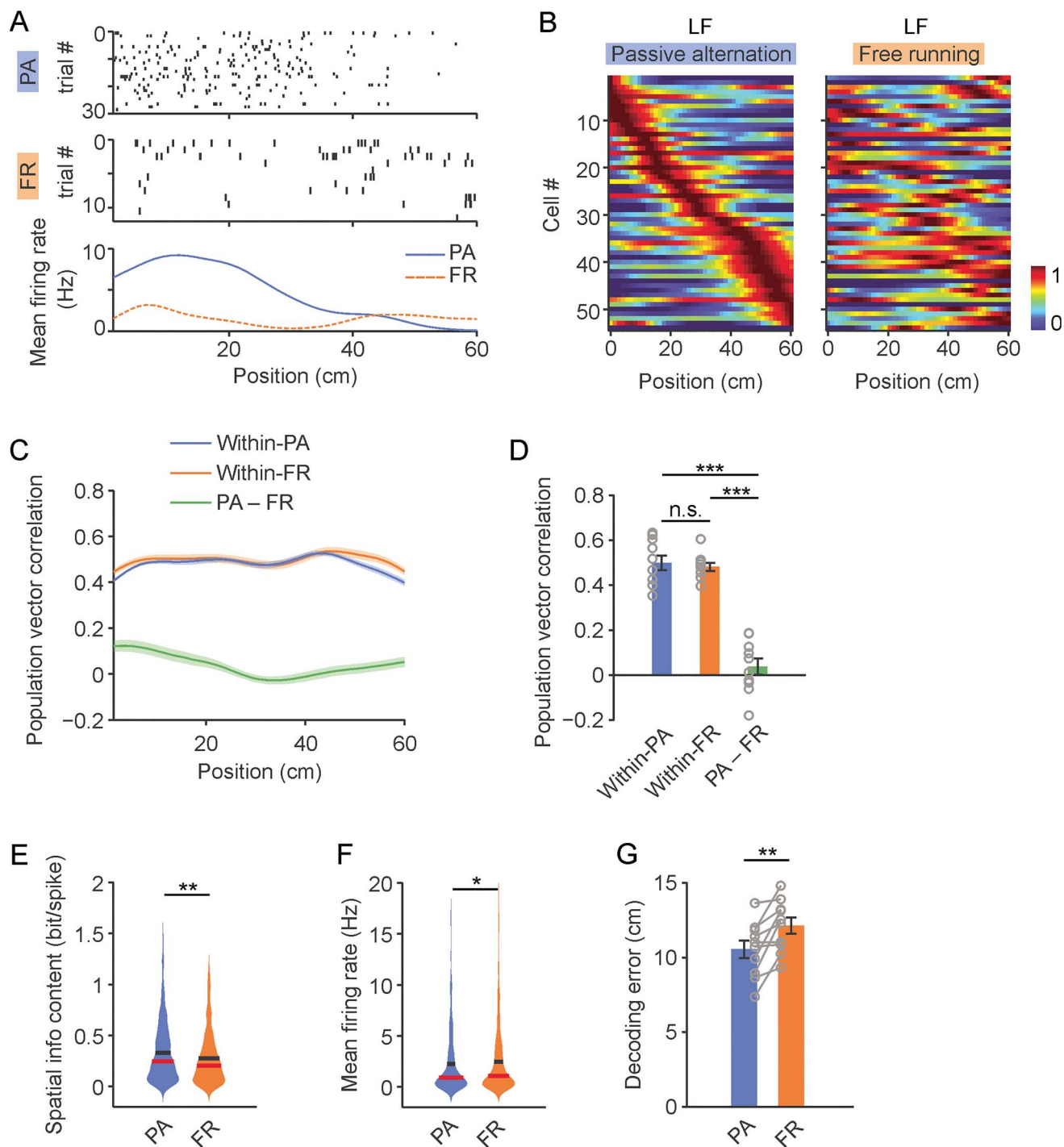


Fig. 5. The effect of reward expectation on the spatial encoding of mPFC neurons. Spatial encoding was compared in neurons tracked in the PA task and free-running (FR). **A**) Representative raster plots of neural spiking (top 2 graphs) and mean firing rate during different tasks (bottom graph) of 1 neuron. X-axis indicates the animal's position represented by the distance to the holding area. **B**) Representative composite firing rate map of all neurons recorded in 1 animal, which are tracked in the PA task and free-running. The cells were ordered by their peak firing locations in the PA task. Color in the firing rate map indicates normalized firing rates. **C**) PVC between different trials of the same task (within-PA and within-free-running) and between the PA task and free-running at each position. Lines indicate the average PVC from 10 sessions from 6 mice. **D**) PVC averaged across all positions for the within-PA, within-free running, and between the PA task and free-running comparison. Each circle represents 1 session; $n = 10$ sessions from 6 mice. **E**) Spatial information content and **F**) mean firing rate of all neurons in designated tasks presented as violin plots illustrating kernel probability density. Red line is median and black line is mean; $n = 313$ neurons from 6 mice. **G**) Decoding error of the PA task and free-running. Each circle represents 1 session; $n = 10$ sessions from 6 mice. Data are presented as mean \pm SEM in **C**, **D** and **G**). * $P < 0.05$, ** $P < 0.01$, and *** $P < 0.001$.

that spatially selective firing of mPFC neurons is task-dependent. The forward and back segments in the free-running task had the same reward status but different running directions. The low PVC between forward and back segments in this task indicates that running direction affects the spatial firing of mPFC neurons.

Although individual mPFC neurons contain spatial information, the spiking activity of multiple neurons encodes the animal location more reliably. The relatively low coding capability of individual mPFC neurons reflects the origin and impact of hippocampal inputs to the mPFC. The mPFC receives monosynaptic inputs from the ventral hippocampus, which is less spatially selective than the dorsal hippocampus (Ciocchi et al. 2015; Chockanathan and Padmanabhan 2021). The ventral hippocampal inputs elicit subthreshold postsynaptic responses in excitatory mPFC neurons (Marek et al. 2018). Moreover, the large amount of non-spatial information relayed to the mPFC by other brain areas may dilute the spatial information sent by the hippocampus.

In all 3 tasks, firing activities at the neural population level encoded the animal location. However, mPFC neural spiking contained a larger amount of spatial information, and the population activity coded animal locations with higher accuracy when the task involved working memory or rewards and when the animal is closer to the reward. Other task-related information such as decision making and confidence of choice may also potentially affect the mPFC location encoding. This is an intriguing topic for future studies.

The acetylcholine and dopamine systems are potentially involved in the mechanism by which reward and working memory enhance mPFC spatial encoding. Acetylcholine plays an important role in arousal, attention, learning, and memory (McGaughy et al. 2002; Conner et al. 2003; Záborszky et al. 2018). Dopamine is involved in motivation, working memory, and reward-related behaviors (Sawaguchi and Goldman-Rakic 1991; Wise 2004; Cohen et al. 2012; Mohebi et al. 2019; Wang et al. 2019; Lee et al. 2021; Tsetsenis et al. 2021). Cholinergic and dopaminergic synapses on pyramidal neurons are widely distributed in the rodent prefrontal cortex (Zhang et al. 2010). The acetylcholine level in the mPFC increases during training for a spatial working memory task, and stimulation of muscarinic M1 receptors in the primate prefrontal cortex modulates working memory performance and neural firing (Teles-Gribo Ruivo et al. 2017; Galvin et al. 2020). The extracellular dopamine level in the monkey dorsolateral prefrontal cortex increases during working memory (Watanabe et al. 1997). Anticipation of foods evokes dopamine efflux in the rat mPFC (Ahn and Phillips 2003). Stimulation of dopamine D1 receptors affects mPFC neural firing (Vijayraghavan et al. 2007). It is possible that cholinergic and dopaminergic transmissions in response to working memory and reward-seeking influence the firing and therefore, spatial encoding in the mPFC.

In sum, our study shows that the population activity of mPFC neurons represents animal location regardless of the involvement of working memory and reward in the task, however, working memory and reward-seeking enhance spatial encoding in the mPFC.

Acknowledgments

We thank George Dold, Bruce Pritchard, David Ide, Danny Trang, Daniel Yochelson, and William Bennett in the Section on Instrumentation, NIMH for building the T-maze and the interface between the T-maze and the electrophysiological recording system. We thank the NIMH IRP Rodent Behavioral Core for support of behavioral analysis. We thank Paul Juneau in the Division of Data Services, NIH Library, Office of Research Services, National Institutes of Health for assistance in statistical analysis. We thank Drs. Ted Usdin and Sarah Williams of the Systems Neuroscience Imaging Resource in the NIMH Intramural Research Program for help with imaging of brain slices. We thank Aishani Shukla from Thomas Sprigg Wootton High School for assistance in the analysis of behavioral data.

Supplementary material

Supplementary material can be found at *Cerebral Cortex* online.

Funding

This work was supported by the Intramural Research Program of the National Institute of Mental Health (1ZIAMH002881 to Z.L., and in part, ZICMH002952).

Conflict of interest statement: The authors declare no conflict of interest.

References

- Ahn S, Phillips AG. Independent modulation of basal and feeding-evoked dopamine efflux in the nucleus accumbens and medial prefrontal cortex by the central and basolateral amygdala nuclei in the rat. *Neuroscience*. 2003;116:295–305.
- Buzsáki G, Moser EI. Memory, navigation and theta rhythm in the hippocampal-entorhinal system. *Nat Neurosci*. 2013;16:130–138.
- Cenquizca LA, Swanson LW. Spatial organization of direct hippocampal field CA1 axonal projections to the rest of the cerebral cortex. *Brain Res Rev*. 2007;56:1–26.
- Chockanathan U, Padmanabhan K. Divergence in population coding for space between dorsal and ventral CA1. *eNeuro*. 2021;8:ENEURO.0211-21.2021.
- Ciocchi S, Passecker J, Malagon-Vina H, Mikus N, Klausberger T. Selective information routing by ventral hippocampal CA1 projection neurons. *Science*. 2015;348:560–563.
- Ciupke SM, Cheng J, Ali YO, Lu HC, Ji D. Progressive functional impairments of hippocampal neurons in a tauopathy mouse model. *J Neurosci*. 2015;35:8118–8131.

- Cohen JY, Haesler S, Vong L, Lowell BB, Uchida N. Neuron-type-specific signals for reward and punishment in the ventral tegmental area. *Nature*. 2012;482:85–88.
- Conner JM, Culbertson A, Packowski C, Chiba AA, Tuszynski MH. Lesions of the basal forebrain cholinergic system impair task acquisition and abolish cortical plasticity associated with motor skill learning. *Neuron*. 2003;38:819–829.
- Csicsvari J, Hirase H, Czurko A, Buzsáki G. Reliability and state dependence of pyramidal cell-interneuron synapses in the hippocampus: an ensemble approach in the behaving rat. *Neuron*. 1998;21:179–189.
- de Saint BP, Hok V, Alvernhe A, Save E, Poucet B. Tagging items in spatial working memory: a unit-recording study in the rat medial prefrontal cortex. *Behav Brain Res*. 2010;209:267–273.
- Dixon ML, Thiruchselvam R, Todd R, Christoff K. Emotion and the prefrontal cortex: an integrative review. *Psychol Bull*. 2017;143:1033–1081.
- Ekstrom AD, Kahana MJ, Caplan JB, Fields TA, Isham EA, Newman EL, Fried I. Cellular networks underlying human spatial navigation. *Nature*. 2003;425:184–187.
- Emondi AA, Rebrik SP, Kurgansky AV, Miller KD. Tracking neurons recorded from tetrodes across time. *J Neurosci Methods*. 2004;135:95–105.
- Euston DR, Gruber AJ, McNaughton BL. The role of medial prefrontal cortex in memory and decision making. *Neuron*. 2012;76:1057–1070.
- Frank LM, Brown EN, Wilson MA. A comparison of the firing properties of putative excitatory and inhibitory neurons from CA1 and the entorhinal cortex. *J Neurophysiol*. 2001;86:2029–2040.
- Fuchs EC, Zivkovic AR, Cunningham MO, Middleton S, LeBeau FEN, Bannerman DMM, Rozov A, Whittington MA, Traub RD, Rawlins JNP, et al. Recruitment of parvalbumin-positive interneurons determines hippocampal function and associated behavior. *Neuron*. 2007;53:591–604.
- Galvin VC, Yang ST, Paspalas CD, Yang Y, Jin LE, Datta D, Morozov YM, Lightbourne TC, Lowet AS, Rakic P, et al. Muscarinic M1 receptors modulate working memory performance and activity via KCNQ potassium channels in the primate prefrontal cortex. *Neuron*. 2020;106:649–661.e4.
- Gemmell C, Anderson M, O'Mara SM. Deep layer prefrontal cortex unit discharge in a cue-controlled open-field environment in the freely-moving rat. *Behav Brain Res*. 2002;133:1–10.
- Granon S, Poucet B. Medial prefrontal lesions in the rat and spatial navigation: evidence for impaired planning. *Behav Neurosci*. 1995;109:474–484.
- Gray C, Maldonado P, Wilson M, McNaughton B. Tetrodes markedly improve the reliability and yield of multiple single-unit isolation. *J Neurosci Methods*. 1995;63:43–54.
- Groenewegen HJ. Organization of the afferent connections of the mediodorsal thalamic nucleus in the rat, related to the mediodorsal-prefrontal topography. *Neuroscience*. 1988;24:379–431.
- Hartley T, Lever C, Burgess N, O'Keefe J. Space in the brain: how the hippocampal formation supports spatial cognition. *Philos Trans R Soc Lond Ser B Biol Sci*. 2014;369:20120510.
- Hok V, Save E, Lenck-Santini PP, Poucet B. Coding for spatial goals in the prelimbic/infralimbic area of the rat frontal cortex. *Proc Natl Acad Sci U S A*. 2005;102:4602–4607.
- Hyman JM, Ma L, Balaguer-Ballester E, Durstewitz D, Seamans JK. Contextual encoding by ensembles of medial prefrontal cortex neurons. *Proc Natl Acad Sci U S A*. 2012;109:5086–5091.
- Jacobs J, Weidemann CT, Miller JF, Solway A, Burke JF, Wei XX, Suthana N, Sperling MR, Sharan AD, Fried I, et al. Direct recordings of grid-like neuronal activity in human spatial navigation. *Nat Neurosci*. 2013;16:1188–1190.
- Jay TM, Witter MP. Distribution of hippocampal CA1 and subicular efferents in the prefrontal cortex of the rat studied by means of anterograde transport of Phaseolus vulgaris-leucoagglutinin. *J Comp Neurol*. 1991;313:574–586.
- Josselyn SA, Tonegawa S. Memory engrams: recalling the past and imagining the future. *Science*. 2020;367:eaaw4325.
- Jung MW, Qin Y, McNaughton BL, Barnes CA. Firing characteristics of deep layer neurons in prefrontal cortex in rats performing spatial working memory tasks. *Cereb Cortex*. 1998;8:437–450.
- Kaefer K, Nardin M, Blahna K, Csicsvari J. Replay of behavioral sequences in the medial prefrontal cortex during rule switching. *Neuron*. 2020;106:154–165.e6.
- Kee SE, Mou X, Zoghbi HY, Ji D. Impaired spatial memory codes in a mouse model of Rett syndrome. *elife*. 2018;7:e31451.
- Kesner RP, Hunt ME, Williams JM, Long JM. Prefrontal cortex and working memory for spatial response, spatial location, and visual object information in the rat. *Cereb Cortex*. 1996;6:311–318.
- Korotkova T, Fuchs EC, Ponomarenko A, von Engelhardt J, Monyer H. NMDA receptor ablation on parvalbumin-positive interneurons impairs hippocampal synchrony, spatial representations, and working memory. *Neuron*. 2010;68:557–569.
- Krettek JE, Price JL. The cortical projections of the mediodorsal nucleus and adjacent thalamic nuclei in the rat. *J Comp Neurol*. 1977;171:157–191.
- Langston RF, Ainge JA, Couey JJ, Canto CB, Bjerknes TL, Witter MP, Moser EI, Moser MB. Development of the spatial representation system in the rat. *Science*. 2010;328:1576–1580.
- Lee JY, Jun H, Soma S, Nakazono T, Shiraiwa K, Dasgupta A, Nakagawa T, Xie JL, Chavez J, Romo R, et al. Dopamine facilitates associative memory encoding in the entorhinal cortex. *Nature*. 2021;598:321–326.
- Ma L, Hyman JM, Durstewitz D, Phillips AG, Seamans JK. A quantitative analysis of context-dependent remapping of medial frontal cortex neurons and ensembles. *J Neurosci*. 2016;36:8258–8272.
- Marek R, Jin J, Goode TD, Giustino TF, Wang Q, Acca GM, Holehonnur R, Ploski JE, Fitzgerald PJ, Lynagh T, et al. Hippocampus-driven feed-forward inhibition of the prefrontal cortex mediates relapse of extinguished fear. *Nat Neurosci*. 2018;21:384–392.
- Mathis A, Herz AV, Stemmler M. Optimal population codes for space: grid cells outperform place cells. *Neural Comput*. 2012;24:2280–2317.
- McGaughy J, Dalley JW, Morrison CH, Everitt BJ, Robbins TW. Selective behavioral and neurochemical effects of cholinergic lesions produced by intrabasalis infusions of 192 IgG-saporin on attentional performance in a five-choice serial reaction time task. *J Neurosci*. 2002;22:1905–1913.
- Miller JF, Neufang M, Solway A, Brandt A, Trippel M, Mader I, Hefft S, Merkow M, Polyn SM, Jacobs J, et al. Neural activity in human hippocampal formation reveals the spatial context of retrieved memories. *Science*. 2013;342:1111–1114.
- Mohebi A, Pettibone JR, Hamid AA, Wong JMT, Vinson LT, Patriarchi T, Tian L, Kennedy RT, Berke JD. Dissociable dopamine dynamics for learning and motivation. *Nature*. 2019;570:65–70.
- Morris RGM, Garrud P, Rawlins JNP, O'Keefe J. Place navigation impaired in rats with hippocampal lesions. *Nature*. 1982;297:681–683.
- Mumby DG, Gaskin S, Glenn MJ, Schramek TE, Lehmann H. Hippocampal damage and exploratory preferences in rats: memory for objects, places, and contexts. *Learn Mem*. 2002;9:49–57.
- Ólafsdóttir HF, Carpenter F, Barry C. Coordinated grid and place cell replay during rest. *Nat Neurosci*. 2016;19:792–794.

- Poucet B. Searching for spatial unit firing in the prelimbic area of the rat medial prefrontal cortex. *Behav Brain Res.* 1997;84:151–159.
- Poucet B, Buhot M-C. Effects of medial septal or unilateral hippocampal inactivations on reference and working spatial memory in rats. *Hippocampus.* 1994;4:315–321.
- Qasim SE, Fried I, Jacobs J. Phase precession in the human hippocampus and entorhinal cortex. *Cell.* 2021;184:3242–3255.e10.
- Ragozzino ME, Detrick S, Kesner RP. Involvement of the prelimbic-infralimbic areas of the rodent prefrontal cortex in behavioral flexibility for place and response learning. *J Neurosci.* 1999;19:4585–4594.
- Rawlins JNP, Olton DS. The septo-hippocampal system and cognitive mapping. *Behav Brain Res.* 1982;5:331–358.
- Sawaguchi T, Goldman-Rakic PS. D1 dopamine receptors in prefrontal cortex: involvement in working memory. *Science.* 1991;256:947–950.
- Skaggs W, McNaughton B, Gothard K. An information-theoretic approach to deciphering the hippocampal code. *Adv Neural Inf Process Syst.* 1992;5:1030–1037.
- Spellman T, Rigotti M, Ahmari SE, Fusi S, Gogos JA, Gordon JA. Hippocampal-prefrontal input supports spatial encoding in working memory. *Nature.* 2015;522:309–314.
- Teles-Griolo Ruivo LM, Baker KL, Conway MW, Kinsley PJ, Gilmour G, Phillips KG, Isaac JTR, Lowry JP, Mellor JR. Coordinated acetylcholine release in prefrontal cortex and hippocampus is associated with arousal and reward on distinct timescales. *Cell Rep.* 2017;18:905–917.
- Towse BW, Barry C, Bush D, Burgess N. Optimal configurations of spatial scale for grid cell firing under noise and uncertainty. *Philos Trans R Soc B Biol Sci.* 2014;369:20130290.
- Tsetsenis T, Badyna JK, Wilson JA, Zhang X, Krizman EN, Subramanian M, Yang K, Thomas SA, Dani JA. Midbrain dopaminergic innervation of the hippocampus is sufficient to modulate formation of aversive memories. *Proc Natl Acad Sci U S A.* 2021;118:e2111069118.
- Uylings HBM, Groenewegen HJ, Kolb B. Do rats have a prefrontal cortex? *Behav Brain Res.* 2003;146:3–17.
- Vijayraghavan S, Wang M, Birnbaum SG, Williams GV, Arnsten AFT. Inverted-U dopamine D1 receptor actions on prefrontal neurons engaged in working memory. *Nat Neurosci.* 2007;10:376–384.
- Wang M, Datta D, Enwright J, Galvin V, Yang ST, Paspalas C, Kozak R, Gray DL, Lewis DA, Arnsten AFT. A novel dopamine D1 receptor agonist excites delay-dependent working memory-related neuronal firing in primate dorsolateral prefrontal cortex. *Neuropharmacology.* 2019;150:46–58.
- Watanabe M, Kodama T, Hikosaka K. Increase of extracellular dopamine in primate prefrontal cortex during a working memory task. *J Neurophysiol.* 1997;78:2795–2798.
- Wilber AA, Skelin I, Wu W, McNaughton BL. Laminar organization of encoding and memory reactivation in the parietal cortex. *Neuron.* 2017;95:1406–1419.e5.
- Wise RA. Dopamine, learning and motivation. *Nat Rev Neurosci.* 2004;5:483–494.
- Yang Y, Mailman RB. Strategic neuronal encoding in medial prefrontal cortex of spatial working memory in the T-maze. *Behav Brain Res.* 2018;343:50–60.
- Yang S-T, Shi Y, Wang Q, Peng J-Y, Li B-M. Neuronal representation of working memory in the medial prefrontal cortex of rats. *Mol Brain.* 2014;7:61.
- Yoon T, Okada J, Jung MW, Kim JJ. Prefrontal cortex and hippocampus subserve different components of working memory in rats. *Learn Mem.* 2008;15:97–105.
- Záborszky L, Gombkoto P, Varsanyi P, Gielow MR, Poe G, Role LW, Ananth M, Rajebhosale P, Talmage DA, Hasselmo ME, et al. Specific basal forebrain-cortical cholinergic circuits coordinate cognitive operations. *J Neurosci.* 2018;38:9446–9458.
- Zhang Z-W, Burke MW, Calakos N, Beaulieu J-M, Vaucher E. Confocal analysis of cholinergic and dopaminergic inputs onto pyramidal cells in the prefrontal cortex of rodents. *Front Neuroanat.* 2010;4:21.
- Zhang L, Ma X, Chen G, Barkai E, Lin L. Theta rhythmic clock-like activity of single units in the mouse hippocampus. *J Neurosci.* 2016;36:4415–4420.
- Zielinski MC, Shin JD, Jadhav SP. Coherent coding of spatial position mediated by theta oscillations in the hippocampus and prefrontal cortex. *J Neurosci.* 2019;39:4550–4565.